

Improved production of $O_2(a^1\Delta)$ in capacitively-coupled radio-frequency discharges

J. W. Zimmerman^a, B. S. Woodard^a, J. T. Verdeyen^b, D. L. Carroll^b,
T. H. Field^b, and W. C. Solomon^a

^aUniversity of Illinois at Urbana-Champaign, Urbana, IL 61820

^bCU Aerospace, Urbana, IL 61820

ABSTRACT

Experimental investigations of radio-frequency discharges in $O_2/He/NO$ mixtures in the pressure range of 1-100 Torr and power range of 0.1-1.2 kW have indicated that $O_2(a^1\Delta)$ production is a strong function of geometry, excitation frequency, pressure and diluent ratio. The goal of these investigations was maximization of both the yield and flow rate (power flux) of $O_2(a^1\Delta)$ in order to produce favorable conditions for application to an electric oxygen-iodine laser (EOIL). At lower pressures, improvements in yield are observed when excitation frequency is increased from 13.56 MHz. As pressure is increased, increasing excitation frequency in the baseline configuration becomes detrimental, and yield performance is improved by reducing the discharge gap and increasing the diluent ratio. Numerous measurements of $O_2(a^1\Delta)$, oxygen atoms, and discharge excited states are made in order to describe the discharge performance dependent on various parameters.

1. INTRODUCTION

The classical chemical oxygen-iodine laser first reported by McDermott¹ operates on the electronic transition of the iodine atom at 1315 nm, $I(^2P_{1/2}) \rightarrow I(^2P_{3/2})$ [denoted hereafter as I^* and I respectively]. The lasing state I^* is produced by near resonant energy transfer with the singlet oxygen metastable $O_2(a^1\Delta)$ [denoted hereafter as $O_2(a)$]. In typical systems, a chemical two-phase process is used to produce the $O_2(a)$ at the interface of liquid basic H_2O_2 and Cl_2 gas. Zaleskii² and Fournier³ made early studies towards using electric discharges for $O_2(a)$ production to pump iodine for lasing, but were unable to obtain positive gain. More recently, various groups⁴⁻⁹ have investigated similar continuous flowing systems and have measured $O_2(a)$ yields in excess of 15%, a necessary condition for positive gain at room temperature. Gain in an electrically-driven system was achieved in work by Carroll *et al.*¹⁰, with lasing in the same system reported in subsequent work¹¹. This system¹¹ made use of a capacitively-coupled longitudinal 13.56 MHz discharge in $O_2:He$ mixtures to provide energy storage in $O_2(a)$. Since this first reporting of a viable electric discharge-driven oxygen-iodine laser system (called EOIL or DOIL in the literature), there have been a number of other successful demonstrations of gain [Rawlins¹², Verdeyen¹³, Hicks¹⁴] and lasing [Verdeyen¹³, Hicks¹⁴]. The highest reported gain to date is 0.10 % cm^{-1} [Benavides¹⁵].

A prominent discharge technique used in EOIL research has been transverse capacitive RF¹⁵⁻²⁰. Experiments and modeling by Rakhimova^{16,17} and Braginsky¹⁸⁻²⁰ have shown that $O_2(a)$ generation in transverse RF discharges is significantly enhanced by exciting the discharge at higher frequencies than the typical 13.56 MHz. Rakhimova¹⁶ suggested that increased frequency led to a narrowing of the sheath region in which $O_2(a)$ production is ineffective and allowed operating the discharge in the homogeneous α -mode to higher energy inputs. Braginsky *et al.*¹⁸ showed that increasing the excitation frequency in a small-diameter transverse discharge (from the typical 13.56 MHz) results in a substantial increase in $O_2(a)$ power efficiency in pure O_2 discharge; with the addition of NO to the mixture and HgO-coated walls, this group obtained $O_2(a)$ yields of ~21% at 10 Torr, ~17% at 20 Torr, and ~13% at 30 Torr using an excitation frequency of 160 MHz¹⁸.

In various works by this group¹⁹, three such operating regimes are identified for different energy deposition modes into the plasma:

- I) Homogeneous mode (α -mode): energy is deposited approximately uniformly across the tube diameter
- II) Transition mode (γ -mode): plasma jets form outside the electrode gap but most of the energy is deposited within the electrode gap.
- III) Inhomogeneous mode: plasma jets and surface wave discharge propagates outside the electrode gap and a large portion of the energy dissipation occurs outside of the gap.

The α -mode is more favorable²⁰ because it results in more efficient energy deposition into O₂(a). However, the maximum O₂(a) production occurs at energy depositions in which the discharge is in γ -mode²⁰. This description of operational mode for flowing RF discharges is consistent with the designations found in non-flowing RF systems first noted by Levitskii²¹. Raizer²² provides numerous examples of this type of behavior in a variety of gas mixtures at moderate pressures (10-100 Torr), the regime of interest in EOIL.

An important characteristic of α -mode RF transverse capacitive discharges is the “normal current density.” In the condition where energy deposition is low and the discharge does not fill the electrode gap, as the current is raised, the discharge volume grows such that the current density remains nearly constant; this constant density is the “normal current density”, sometimes denoted $j_{n\alpha}$ (see Raizer²²). From work by Yatsenko²³ with He and Air discharges, the following trends can be expected: (1) $j_{n\alpha}$ varies with mixture, (2) $j_{n\alpha}$ increases with pressure, (3) $j_{n\alpha}$ increases with gap. Carroll *et al.*¹¹ suggested that the increase in O₂(a) production from the presence of NO in the discharge gas mixture that they first observed¹¹ is due to a lower ionization potential of NO thereby enhancing the electron number density in the discharge which results in better discharge stability and increased pumping of the O₂(a). Braginsky *et al.*¹⁸ expand on this idea by suggesting that the beneficial influence arises from the lower ionization potential gas mixture leading to the plasma occupying more volume within the gap, thus lowering the normal current density¹⁸.

Vidaud²⁴ experimented with α to γ transition and found that transition voltage increases with increasing pressure, and decreases with increasing frequency. Odrobina²⁵ modeled the transition between α and γ mode and showed that increasing the applied frequency led to a decrease in the sheath depth and delayed the transition to higher energy deposition, consistent with Rakhimova's conclusions for the flowing system¹⁶; Odrobina²⁵ also found that transition voltage decreased as frequency increased, consistent with Vidaud's observations.

In 2-D modeling work, Rakhimova *et al.*¹⁷ showed that when the discharge frequency was increased from 13.56 to 81 MHz for an energy deposition range of 50-400 J/mmol, the discharge spatial structure changed dramatically. The case modeled was 10 Torr of pure oxygen in a transverse discharge with 14-mm gap and 30-cm electrode length. At 13.56 MHz, the discharge glow filled the electrode gap, and the power was uniformly deposited¹⁷. In the 81 MHz case, the discharge did not fully occupy the discharge gap, and the discharge operated in normal current density mode¹⁷. In the modeling result, the length occupied by the 81 MHz discharge increased with energy deposition, which was in good agreement with visual observation of the experiment¹⁷. Also, the electron density, and specific energy input (per unit volume) in the 81 MHz case were twice as high as the 13.56 MHz case¹⁷.

In this paper, behaviors of typical ElectricOIL transverse RF discharges in O₂:He:NO mixtures are discussed, showing the influence of frequency on O₂(a) and oxygen atom production in the pressure range of 1-100 Torr. The transition between α and γ modes is described, and the influence of frequency on discharge structure and electron density is established via experimental measurements of discharge intensity. It is shown that increased yield can be obtained at moderate pressures (20-30 Torr) by increasing the excitation frequency and reducing the discharge gap, following the behaviors observed and modeled by Rakhimova^{16,17} and Braginsky¹⁸⁻²⁰ for pure oxygen and O₂:NO mixture. The influence of frequency on the discharge characteristics is shown using spatial measurements of the Herzberg I and II bands in O₂. Measurements of oxygen atoms, using actinometry within the discharge, and O-NO recombination in the discharge afterglow are reported for a variety of configurations and flow conditions. The general trends observed are as follows:

- i) At the low end of the pressure range, increasing the excitation frequency (from 13.56 MHz) leads to increased O₂(a) production; at high pressures increasing the excitation frequency (from 13.56 MHz) is detrimental to O₂(a) production.
- ii) For fixed geometry, power input, and frequency, there is an optimal operating pressure at which the O₂(a) yield is maximized. As the frequency is increased, the optimal pressure decreases. As the discharge gap decreases, the optimal pressure increases.
- iii) O₂(a) yield in the afterglow for the conditions studied is maximized by operating at low pressure and high frequency.

- iv) The excitation frequency has a significant impact on the spatial characteristic behavior of the discharge with measurements suggesting that increasing frequency leads to higher electron density, and operation in α -mode to higher energy deposition (similar to Rakhimova's results^{16,17}). This leads to higher power densities and higher dissociation fractions; decreasing the discharge volume has the same effect.
- v) Addition of trace amounts of NO to the mixture increases the O₂(a) yield significantly over the entire pressure range.
- vi) At high pressures, increasing the He diluent ratio leads to significant boosts in O₂(a) yield.

2. EXPERIMENTAL APPARATUS

2.1 Discharge configurations and flow system

For purposes of this paper, the results from four transverse capacitive RF discharge geometries will be discussed. These are summarized in Table 1. All four discharges use 25.4-cm long (10") copper plates or foil as electrodes. The term "clamshell" is used to describe a set of transverse electrodes which conform to the outer radius of the tube. The discharges were excited with (RF) power at 13.56, 27.12, and 60 MHz. The power supplies used in these studies are described in Table 2. The ENI A-1000 variable frequency power supply was driven with a Wavetek model 164 wave generator. Incident and reflected powers to the radio-frequency (RF) matching network were measured by a Bird ThruLine model 43 wattmeter (RF "System Power" is the difference of the incident and reflected powers). Matching of the power to the discharge was achieved using a traditional PI-matching network designed for each frequency. Voltage and currents were measured with a Tektronix model P6015 high-voltage probe (or a capacitive pick-up calibrated to this probe) and Pearson model 411 current monitors.

Table 1. Transverse RF Discharge Geometries.

#	Flow Tube, Electrodes	Max. Internal Gap [cm]	Internal Volume [cm ³]	Wall thickness [cm]
1	Circular, "Clamshell"	4.9 cm	479	0.25
2	Circular, Parallel Plate	4.9 cm	479	0.25
3	Rectangular, Parallel Plate	3.0 cm	465	0.30
4	Circular, Parallel Plate	2.0 cm	77.4	0.15

Table 2. RF Power Supplies.

#	Manufacturer	Model #	Frequency Range	Power Range
1	ENI	OEM-12A	13.56 MHz, fixed	1 kW
2	ENI	OEM-25A	13.56 MHz, fixed	2.5 kW
3	ENI	A-1000	0.3-35 MHz	~1 kW @ 27 MHz
4	Comdel	CPS-1001	60 MHz, fixed	1.25 kW

Micro-Motion CMF and Omega FMA mass flow meters were used to measure the flow rates of the gases. Pressures in the flow tubes were measured with MKS Instruments transducers. The flow setups used in this study are sketched in Figure 1.

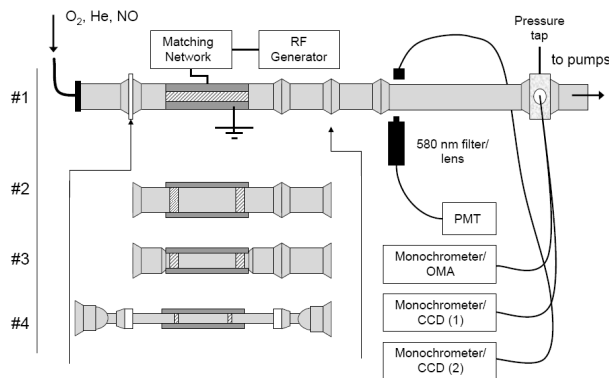


Figure 1. Sketches of experimental flow setups.

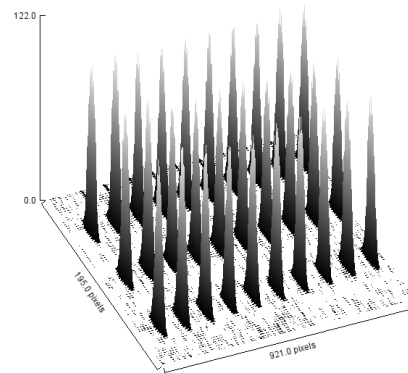
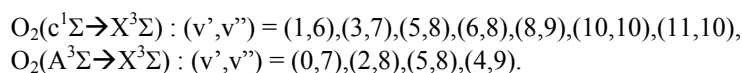


Figure 2. Sample measurement of Herzberg I and II bands in discharge geometry #3.

2.2 Diagnostics suite for excited oxygen, and oxygen atom measurements

A Princeton Instruments/Acton Optical Multi-channel Analyzer (OMA-V, 1024-element InGaAs array) with a 0.3-m monochromator and a 600 g/mm grating blazed at 1 μm was used for measurements at 1268 nm. An Apogee E47 CCD camera coupled to a Roper Scientific/Acton Research 150-mm monochromator (1) was used to measure the emission of $\text{O}_2(\text{b})$ at 762 nm to determine flow temperature, as well as the emissions of excited atomic oxygen at 777 nm, and excited argon at 750.4 and 751.5 nm. A Santa Barbara Instruments Group CCD with an Acton 150-mm monochromator (2) was also used to measure $\text{O}_2(\text{b})$. The broadband emission of NO_2^* was measured using a Hamamatsu R955 photomultiplier with a narrowband 580 nm filter and a 50 mm focal length collection lens; the O-atom concentration was determined from NO_2^* using the method described by Piper²⁶. These optical diagnostics were fiber coupled using either Oriel model #77538 glass fiber bundles or ThorLabs 600 μm x 5 m multimode fibers.

The measurement of the Herzberg I and II band groups²⁷ in O_2 was accomplished using a Nikon D70 with narrowband 404.7 nm filter placed in the optical path. The filter has a 11-nm bandwidth (399-410 nm), which allows capture of



The camera was set up such that the optical axis was perpendicular to the grounded plate of discharge configuration #3, such that the O_2^* emission from 0.125" holes in the plate could be collected. Typical 404.7 nm emission data is shown in Fig. 2 for a case in which the excitation is uniform.

3. EXPERIMENTAL RESULTS

3.1 $\text{O}_2(\text{a})$ and O-atom results in baseline configuration (20, 30 and 50 Torr)

At higher operating pressures, the $\text{O}_2(\text{a})$ decays significantly with distance from the electrode gap. Figure 3 shows the decay of $\text{O}_2(\text{a})$ yield in the afterglow of discharge geometry #1 for operation at 800 W in a mixture of 10:33:0.15 mmol/s O_2 :He:NO at 20, 30 and 50 Torr. Here the " $\text{O}_2(\text{a})$ Yield" is defined as $[\text{O}_2(\text{a})]/[\text{O}_2]_{\text{input}}(T,p)$, where $[\text{O}_2]_{\text{input}}(T,p)$ is the total input O_2 density evaluated at the local measured temperature T and pressure p. The exit yields for these cases are ~16% at 20 Torr, ~14% at 30 Torr, and ~6% at 50 Torr; the slope of yield with distance is similar for the three pressures. Figure 4 shows the decay of the oxygen atom yield with distance for the cases shown in Fig. 3; the oxygen atom yields were determined from O-NO recombination measurement at 580-nm.

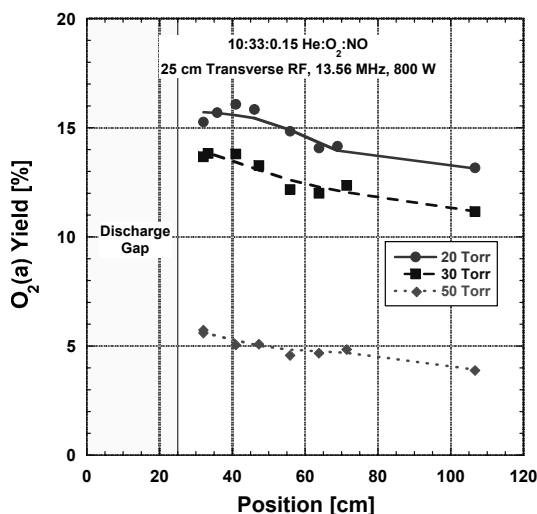


Figure 3. $\text{O}_2(\text{a})$ yield vs. position downstream of discharge geometry #1 for 10:33:0.15 mmol/s O_2 :He:NO at 20, 30 and 50 Torr.

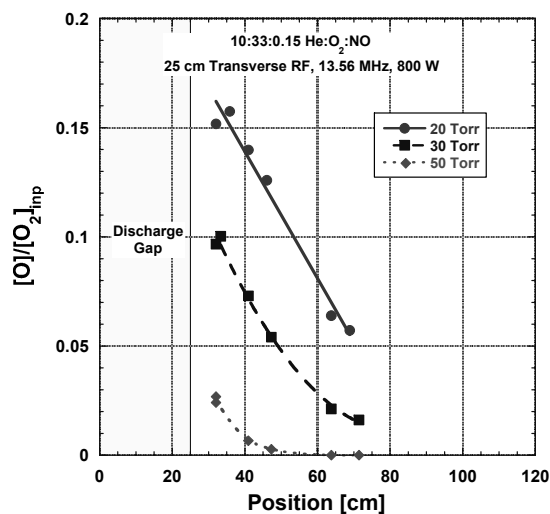


Figure 4. Oxygen atom yield vs. position downstream of discharge geometry #1 for 10:33:0.15 mmol/s O_2 :He:NO at 20, 30 and 50 Torr.

3.2 α to γ Transition in a 13.56 MHz Discharge in O_2 :He Mixture

To show the transition between α to γ modes in a typical ElectricOIL discharge setup, the current-voltage-characteristic (CVC) was taken for discharge geometry #3 at the baseline flow rate of 10:33 O_2 :He at ~ 21 Torr without, and with a trace NO flow rate of 0.15 mmol/s. As seen in Figure 5a, at low input powers, the discharge operates in homogeneous α -mode. As power is increased, the current increases, and there is a transition in the neighborhood of 1.7-1.9 A, after which the voltage and current both increase with increased power input. As will be shown later, this transition point occurs at nearly the same RF power input where the plates are nearly filled with plasma, and that beyond this power, the electron density (and therefore current density) increases throughout the electrode gap region. The trace NO flow rate has little effect on the transition point which occurs at approximately 350 W RF. However the production of $O_2(a)$ increases significantly. Figure 5b shows $[O_2(a)]$ determined from 1268-nm emission measured 58 cm downstream of the electrode gap for the cases in Fig. 5a. In the α -mode, $[O_2(a)]$ increases linearly with RF power; as more power is added, there is a transition to γ -mode and the slope in $[O_2(a)]$ vs. RF decreases. The addition of NO results in an increase of the slope in $[O_2(a)]$ vs. RF in the α -mode; because the CVC is not substantially affected by the addition of trace NO, it appears that the beneficial increase in $O_2(a)$ is due primarily to a kinetic effect and not due to the influence of the lower ionization potential of NO. Figure 6 shows the influence of pressure on the CVC for 10:33 mmol/s O_2 :He. As pressure is increased, the transition voltages and currents increase. For the 32 Torr case in Fig. 6, it was trivial to operate the discharge in either α or γ -mode at powers near 500 W (2.8-3.4 A) by careful matching of the discharge as this transition point was approached from high (γ -mode) or low (α -mode) powers; thus, a significant amount of overlap in the two modes is observed in the CVC. Similar hysteretic behaviors near transition were observed in work by Vidaud²⁴. The maximum yield does not necessarily occur in γ -mode; for instance, the yield for the 50 Torr case shown in Fig. 3 saturated with the discharge in α -mode.

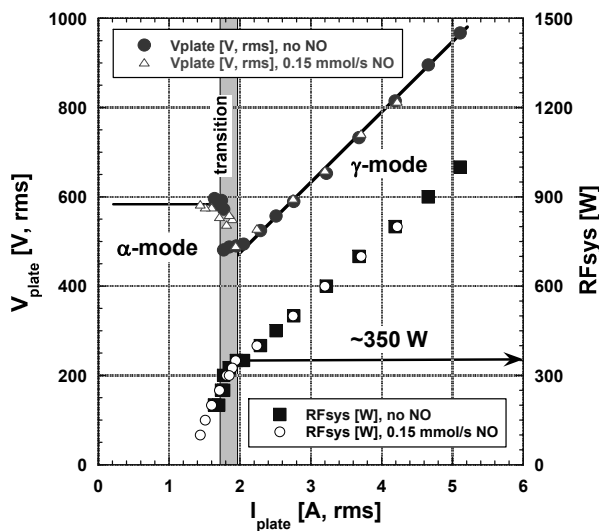


Figure 5a. Current-voltage characteristic and current power characteristic in discharge geometry #3 for 10:33 O_2 :He at ~ 21 Torr +/- 0.15 mmol/s NO. The transition to γ -mode occurs at ~ 350 W RF input in either case.

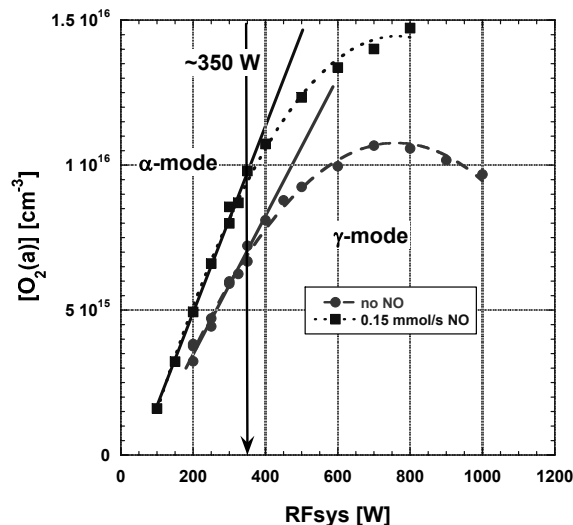


Figure 5b. $[O_2(a)]$ measured 58 cm downstream of discharge geometry #3 for 10:33 O_2 :He at ~ 21 Torr +/- 0.15 mmol/s NO. The transition to γ -mode occurs at ~ 350 W RF input in either case.

3.3 Excitation frequency influence on $O_2(a)$ and O-atom production

Figure 7 shows $O_2(a)$ yield as a function of pressure without and with NO for 13.56 MHz and 60 MHz in discharge geometry #3 (rectangular tube). These measurements were made 89 cm downstream of the discharge gap in a 50-mm I.D. circular flow channel, and therefore the curves are distorted from the exit yield by increasing $O_2(a)$ decay as pressure is increased. It was necessary to make measurements at this downstream location in order to have direct yield comparisons over the range of discharge tube geometries; the transition between the smaller diameter tubes and the 50-mm I.D. (well-calibrated) diagnostic block volume results in a subsonic jetting effect (highly visible via O-NO recombination emission) which confuses interpretation of the measured 1268-nm intensity due to axial

variations of flow parameters. The influence of frequency on $O_2(a)$ production is substantial, and has no characteristic dependence on trace NO content. At 5 Torr (low pressure), the yield increases by more than a factor of two when frequency is increased from 13.56 to 60 MHz, reaching a maximum of 18%; near 20 Torr, the production level of $O_2(a)$ is nearly identical at the two frequencies; at pressures greater than 20 Torr, the use of the higher frequency results in strong reduction in $O_2(a)$ levels and it is better to use a 13.56 MHz discharge at pressure > 20 Torr for this particular geometry. This data suggests a strong coupling between the influences of discharge pressure and excitation frequency on discharge behavior. Rahkimova et al.¹⁶ observed improved $O_2(a)$ yield at 30 Torr by increasing excitation frequency from 13.56 MHz to 81 and 160 MHz, but this may be explained by the fact that they took their 80 MHz data with a $\frac{1}{2}$ " (14 mm) diameter discharge tube and the 160 MHz data with a $\frac{1}{4}$ " (7 mm) discharge tube, which allowed extension of $O_2(a)$ production efficiency to higher pressures.

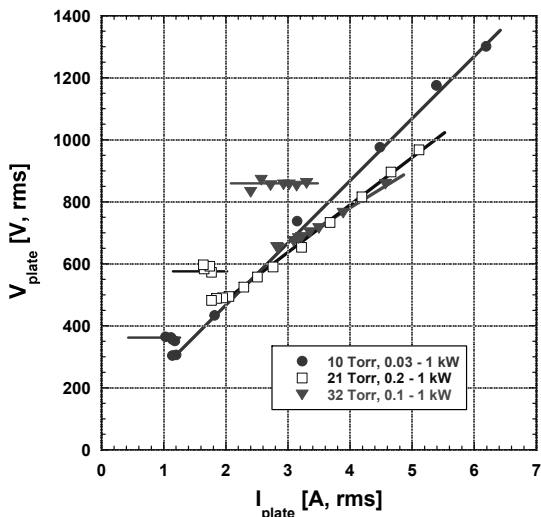


Figure 6. Current-voltage characteristic in discharge geometry #3 for 10:33 $O_2:He$ with varied pressure. The transition voltage and current increase with increasing pressure.

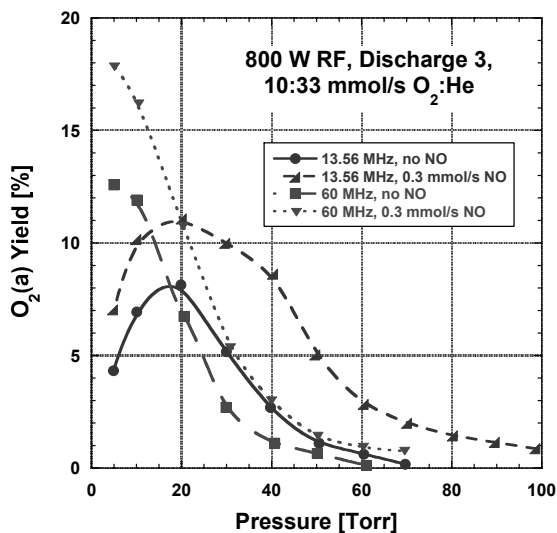


Figure 7. $O_2(a)$ yield as a function of pressure for varied excitation frequency in discharge geometry #3 (rectangular). Data measured 89 cm from discharge exit.

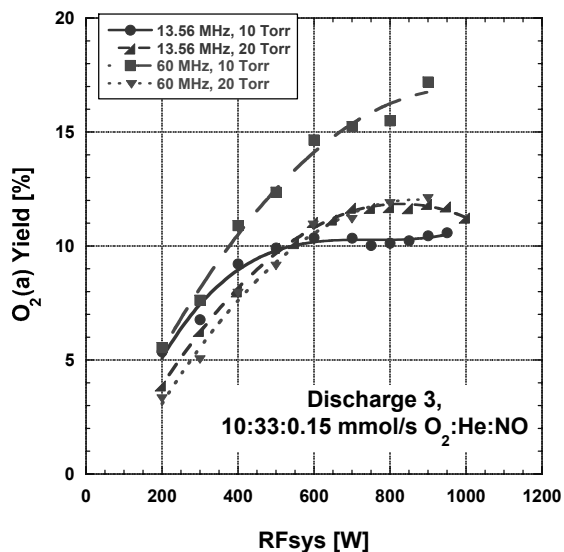


Figure 8. $O_2(a)$ yield as a function of power at 10 and 20 Torr for varied excitation frequency in discharge geometry #3 (rectangular). Data measured 89 cm from discharge exit.

Figure 8 shows the influence of excitation frequency on $O_2(a)$ yield as a function of power in discharge geometry #3 for 10:33:0.15 mmol/s $O_2:He:NO$ at 10 and 20 Torr. The $O_2(a)$ production is similar for the two frequencies at 20

Torr; at 10 Torr, the slope of yield with power is significantly increased. Given the similarity seen in Figures 7 and 8 for the 20 Torr cases at 800 W, one might expect the discharge characteristics to also be similar. However, this is not the case, and the discharge structure is quite different at the two frequencies. As will be shown, the 60 MHz case operates in α -mode while the 13.56 MHz case is in γ -mode.

The increase in frequency also results in a significant increase in oxygen atom production due to the larger power density. The oxygen atom content determined by O-NO recombination emission at 580-nm is shown in Fig. 9 as a function of (a) RF input power and (b) pressure. At the measurement position (46 cm from the exit), the oxygen atoms are nearly completely recombined for pressures of 30 Torr and greater. However, the increase in dissociation due to frequency is substantial for the variety of cases shown; increasing the frequency to 60 MHz results in the discharge being either (1) shifted to α -mode from γ -mode (typical low pressure case) or (2) constricted in α -mode to higher current density operation (typical high pressure case). In either situation, the current density is increased, and therefore oxygen dissociation increases.

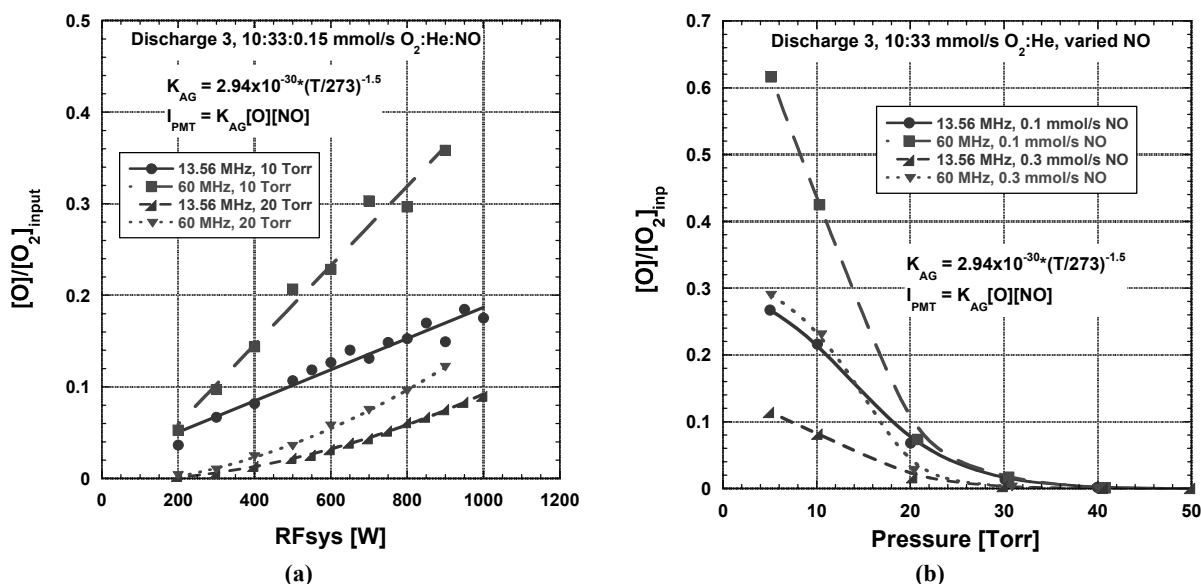


Figure 9. The influence of frequency and oxygen atom production. The airglow emission due to O-NO recombination was measured 46 cm downstream using a PMT filtered at 580 nm: (a) oxygen atom yield vs. RF input power for varied frequency and pressure, and (b) oxygen atom yield vs. pressure for varied frequency and NO content.

Decreasing the discharge gap (and volume) led to enhanced O₂(a) production at mid-range pressures (20-70 Torr). Figures 10 and 11 summarize data taken with discharge configuration #4 (circular, small diameter). Although the behavior with pressure and frequency is similar to that seen in Fig. 7, the use of a smaller discharge gap resulted in an extension of the benefit of frequency to higher pressures. At an operating pressure of 20 Torr, increasing the excitation frequency from 13.56 MHz to 60 MHz doubled the O₂(a) production; O₂(a) yield > 15% was obtained for the 60 MHz case. This result is consistent with Rakhimova's work¹⁶ in which it was necessary to lower the tube diameter as the frequency increased to maximize O₂(a) production.

The increased frequency led to similar changes in oxygen atom production in both geometries #3 and #4; Figure 12 shows the actinometry measurements comparing oxygen atom yield at 800 W RF in discharge geometries #3 and #4 for 13.56 and 60 MHz. The significant increase in power density (W/cm³) between geometries #3 and #4 results in a substantial increase in the dissociation. For geometry #3, the higher power volume at 60 MHz compared to that at 13.56 MHz results in the slope of dissociation fraction increasing by a nearly factor of 6; in the smaller diameter tube (geometry #4) the slope of atom production at 13.56 and 60 MHz is similar, which is likely due to the power densities being similar in this case; however, the O-atom level is higher at the discharge exit for the 60 MHz case.

As shown in Fig. 13, the $O_2(a)$ yield was increased at high pressure by increasing the diluent ratio; ~13% yield was obtained at 50 Torr exciting the small diameter discharge (geometry #4) at 27 MHz.

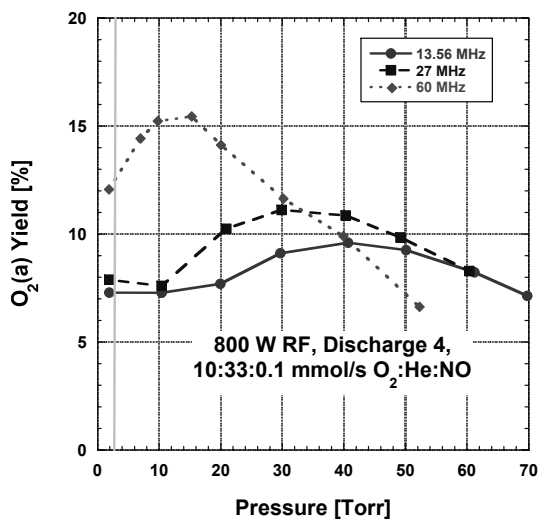


Figure 10. $O_2(a)$ yield as a function of (diagnostic block pressure) for varied excitation frequency at 800 W in discharge geometry #4 (circular, small diameter). Data measured 89 cm downstream from the discharge exit. The cases to the left of the vertical line at ~3 Torr correspond to cases in which the discharge pressure is higher than the diagnostic-block pressure.

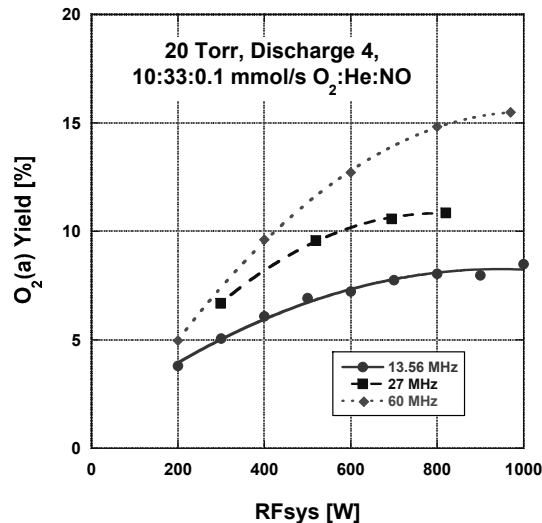


Figure 11. $O_2(a)$ yield as a function of power for varied excitation frequency at 20 Torr in discharge geometry #4 (circular, small diameter). Data measured 89 cm downstream from the discharge exit.

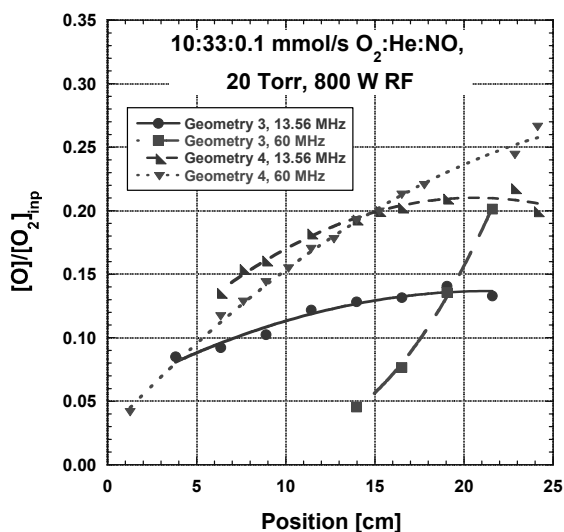


Figure 12. Argon actinometry results for oxygen atom yield in discharge geometries #3 and #4. Measurements made inside the discharge region.

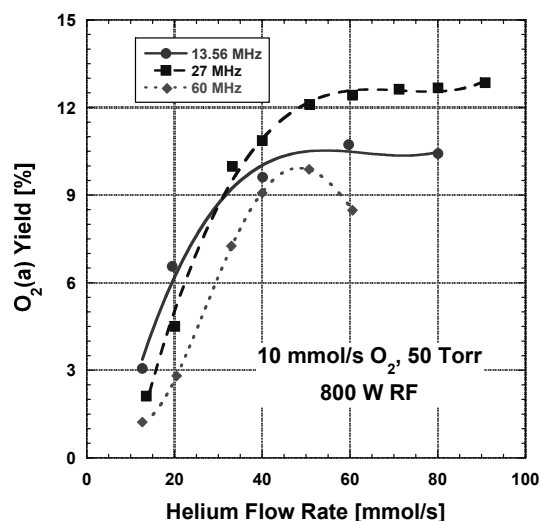


Figure 13. $O_2(a)$ yield as a function of helium diluent for varied excitation frequency at 50 Torr in discharge geometry #4 (circular, small diameter). Data measured 89 cm downstream from the discharge exit.

3.4 Spatial measurements of excited O_2 (Herzberg I and II bands)

The modal behavior of the discharge can be observed qualitatively by visual inspection of the various discharge glow emissions and the air-glow ($O-NO \rightarrow NO_2^* \rightarrow NO_2 + hv$) in the various cases with NO added to the flow. Figure 14 shows photographs of discharge geometry #2 driven at 13.56 MHz with a flow mixture of 10:33:0.15

O₂:He:NO at 20 and 50 Torr for a variety of power levels. As the power is increased, the fraction of the plate gap occupied by the plasma emission is increased. For the 20 Torr case, with power increasing from 0.2 to 1 kW, transition of the discharge from α to γ -mode is observed; when the pressure is increased to 50 Torr, α -mode is maintained up to 1 kW. The spatial behavior of the discharge in the smaller 2.0 cm diameter tube is quite different than the results seen for the 5 cm I.D. tube; as seen in Fig. 15, the visible plasma fills the electrode gap completely for 50 Torr and 800 W RF. The glow visible downstream of the discharge gap in Figs. 14 and 15 is due to O-NO recombination.

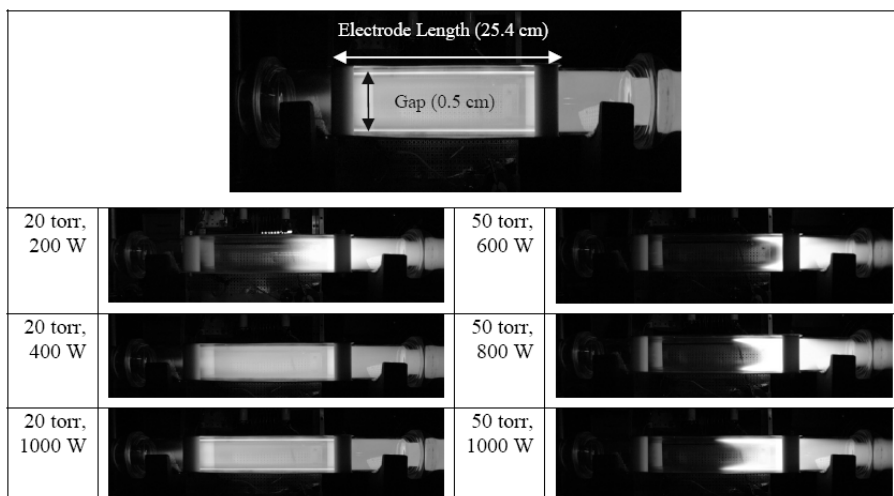


Figure 14. Photographs of discharge glow in geometry #2 (circular, 4.9 cm diameter) at 13.56 MHz. The flow mixture was 10:33:0.15 mmol/s O₂:He:NO.

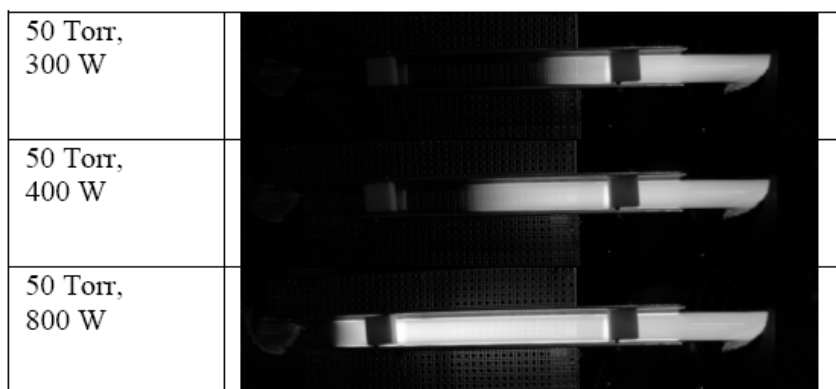


Figure 15. Photographs of discharge glow in geometry #4 (circular, 2.0 cm diameter) at 13.56 MHz. The flow mixture was 10:33:0.15 mmol/s O₂:He:NO.

This visualization is a good qualitative technique for discerning the volume occupied by the plasma between the plates, but it does not directly describe the discharge characteristics (n_e , T_e or E/N). Also, it does not allow the influence of trace NO on the plasma volume to be deduced. In order to determine the influence of frequency on the discharge characteristics, O₂(A³ Σ \rightarrow X³ Σ) and O₂(c¹ Σ \rightarrow X³ Σ) transitions were monitored (Herzberg I and II band groups). A 404.7 nm filter with an 11-nm bandwidth was used, capturing a number of transitions in each band group. For fixed mixture and pressure, and assuming that the pumping rate is unaffected by frequency (i.e. EEDF is similar) the intensity of this state should be proportional to the electron density.

The 404.7 nm intensity measurement as a function of position and power from discharge geometry #3, comparing 13.56 and 60 MHz at 20 Torr, is shown in Fig. 16a. Figure 16b shows some cross-sections of this data for fixed

power and pressure. The intensity was deduced from the average of the filtered emission from three evenly spaced span-wise rows of 1/8" holes in the grounded electrode. In the 13.56 MHz case at high power, the visible plasma fills the electrode gap and the intensity is relatively constant, falling off with distance as the gas is heated through the discharge. For the same input conditions at 60 MHz, the intensity increases greatly at nearly the mid-point of the electrode gap and reaches a level in excess of the 13.56 MHz case. This data indicates that increasing the frequency from 13.56 MHz results in both higher electron density and higher current density (since the visible plasma is confined downstream at higher frequency). In the lower pressure case (10 Torr), this effect results in enhanced O₂(a) production. At 20 Torr, there is no benefit in O₂(a) production for increased frequency, although the influence of frequency on discharge character is similar. The significant increase in electron density and decrease in plasma volume with frequency agrees well with Rakhimova *et al.*'s modeling result¹⁷ which showed that increasing the frequency allows the discharge to operate in α -mode to higher energy deposition. Clearly, operating discharge geometry #3 at higher frequency results in α -mode operation at a higher current density for a given energy deposition, and transition is delayed to higher energy depositions.

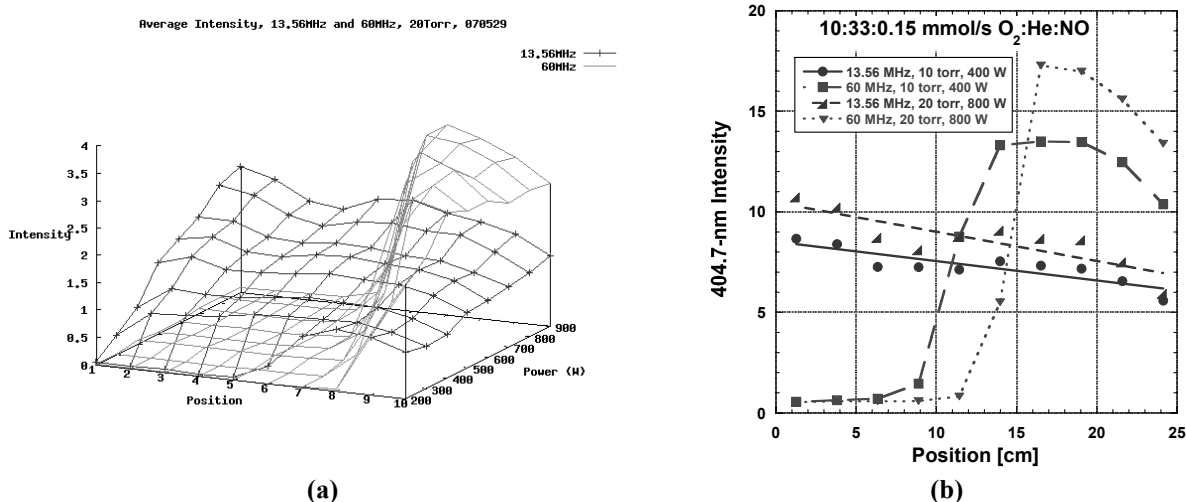


Figure 16. 404.7-nm intensity as a function of position and RF input power for varied excitation frequency in discharge geometry #3 (rectangular): (a) Intensity = $f(\text{position, RF input})$ for 10:33:0.15 mmol/s O₂:He:NO at 20 Torr, (b) Intensity = $f(\text{position})$ for 10:33:0.15 mmol/s O₂:He:NO at 10 and 20 Torr with 40 W/Torr input RF power.

4. SUMMARY

The region of high yield operation was extended to higher pressures by following the pd scaling laws exemplified by Rakhimova *et al.*¹⁶⁻²⁰, showing improved operation by decreasing the tube diameter while increasing the excitation frequency. The transition between α and γ modes was established by CVC (current-voltage-characteristic) measurements; measurements of O₂(a) in afterglow clearly indicate the reduction in O₂(a) production efficiency after transition, although the peak yield occurred at higher energy deposition in γ -mode. The addition of trace NO leads to no clear change in the CVC, but results in a large increase in O₂(a) yield (as shown in earlier works^{10,11,28}), and the slope [O₂(a)] with RF power input in α -mode.

The increase in transition power deposition with increasing pressure was observed for typical laser flow rates, with the transition corresponding to the point at which the plasma fills the electrode gap; the transition voltage and current increased with pressure. Therefore, at a given power level (sufficiently high for γ -mode operation at low pressure), as pressure is increased, there is a critical operating pressure at which the transition back into the α -mode will occur.

The level of O₂(a) produced for a given discharge geometry, mixture, power input, and excitation frequency is a strong function of pressure. At low pressure, γ -mode operation, increasing the excitation frequency trends toward α -mode operation, which leads to higher production efficiency of O₂(a) for a given energy deposition. At mid range to high pressures beyond the critical (transition) pressure, where the discharge is in α -mode, increasing the frequency

leads to further constriction of the discharge to high normal current density, which results in higher dissociation and lower O₂(a) yield in the afterglow, perhaps due to increased quenching.

When the discharge diameter (and volume) is decreased, the transition between α and γ modes occurs at lower power input, and the critical pressure associated with transition between γ -mode (at low pressure) and α -mode (at high pressure) increases. As a result increasing the discharge frequency in the smaller volume discharge (geometry #4) is effective in increasing O₂(a) production at higher pressures compared to the larger volume case (geometry #3).

Based on these results, it is the goal of future work to pursue a transverse RF discharge design in which more efficient O₂(a) production is achieved by maintaining the α -mode to high power inputs. Increasing the excitation frequency at low pressures has allowed maintenance of α -mode to higher energy depositions, resulting in enhancement of the O₂(a) yield. In the high pressure case, which is more desirable for ElectricOIL operation, the influence of frequency is reversed, and it is necessary to decrease the discharge gap in order to exploit the benefit of higher frequency operation, or to operate at lower frequency. In any case, operation of the discharge at higher specific power (power per volume) results in increased oxygen atom production leading to higher quenching of O₂(a). Therefore, if it is necessary to reduce the gap to maintain favorable O₂(a) production at higher pressure, this may be accomplished by reducing the transverse gap while maintaining the volume between the electrodes such that low power density is maintained.

ACKNOWLEDGEMENTS

This work was supported by the Joint Technology Office (JTO) through the Air Force Office of Scientific Research (AFOSR), and the Missile Defense Agency (MDA) through the U.S. Army Space and Missile Defense Command (USA SMDC). The authors acknowledge the contributions of: W.T. Rawlins and S.J. Davis (Physical Sciences Inc.); M. Heaven (Emory Univ.); M. Kushner (Iowa St. Univ.); G. Perram (Air Force Institute of Tech.); M. Berman (AFOSR); B. Otey (USA SMDC); D.A. Hostutler (AFRL); Lt. Col. W. Fink (JTO); J. Kotora and D. Podolski (MDA); G.W. Sutton (Sparta Inc.); and T. Rakhimova and O. Proshina (Lomonosov Moscow State Univ.).

REFERENCES

1. W. McDermott, N. Pchelkin, D. Benard, and R. Bousek, *Appl. Phys. Lett.* **32** (8) 469 (1978).
2. Zalesskii, V. Yu., *Zh. Eksp. Teor. Fiz.*, **67** 30 (1974) [*Sov. Phys. JETP* **40** (1) 14 (1975)].
3. G. Fournier, J. Bonnet, and D. Pigache, *J. Physique* **41** Colloque C9, 449 (1980).
4. D.L. Carroll, J.T. Verdeyen, D.M. King, B.S. Woodard, L.W. Skorski, J.W. Zimmerman, and W.C. Solomon, *IEEE J. Quant. Elect.* **39** (9) 1150 (2003).
5. D.L. Carroll, J.T. Verdeyen, D.M. King, B.S. Woodard, J.W. Zimmerman, L.W. Skorski, and W.C. Solomon, "Recent Experimental Measurements of the ElectricOIL System," AIAA Paper 2003-4029 (2003).
6. J. Schmiedberger, S. Hirahara, Y. Ichinoche, M. Suzuki, W. Masuda, Y. Kihara, E. Yoshitani, and H. Fujii, *SPIE* Vol. **4184**, 32 (2001).
7. A.E. Hill, in *Proc. of the International Conf. on Lasers 2000*, ed. by V. Corcoran and T. Corcoran (STS Press, McClean, VA) 249 (2001).
8. A.A. Ionin, Y.M. Klimachev, A.A. Kotkov, I.V. Kochetov, A.P. Napartovich, L.V. Seleznev, D.V. Sinityn, and G.D. Hager, *J. Phys. D: Appl. Phys.* **36** 982 (2003).
9. T.V. Rakhimova, A.S. Kovalev, A.T. Rakhimov, K.S. Klopovsky, D.V. Lopaev, Y.A. Mankelevich, O.V. Proshina, O.V. Braginsky, and A.N. Vasilieva, "Radio-Frequency Plasma Generation of Singlet ($a^1\Delta_g$) Oxygen in O₂ and O₂:Ar (He) Mixtures," AIAA Paper 2003-4306 (2003).
10. D.L. Carroll, J. T. Verdeyen, D. M. King, J. W. Zimmerman, J. K. Laystrom, B. S. Woodard, N. Richardson, K. Kittell, M.J. Kushner, and W. C. Solomon, "Measurement of positive gain on the 1315 nm transition of atomic iodine pumped by O₂($a^1\Delta$) produced in an electric discharge," *Appl. Phys. Lett.*, **85** (8) 1320-1322 (2004).

11. D.L. Carroll, J. T. Verdeyen, D. M. King, J. Zimmerman, J. Laystrom, B. Woodard, G. Benavides, K. Kittell, D. Stafford, M. J. Kushner, and W. C. Solomon, "Continuous-wave laser oscillation on the 1315 nm transition of atomic iodine pumped by $O_2(a^1\Delta)$ produced in an electric discharge," *Appl. Phys. Lett.*, **86**, 111104 (2005).
12. Rawlins, W.T., Lee, S., Kessler, W.J., and Davis, S.J., "Observations of Gain on the $I(^2P_{1/2} \rightarrow ^2P_{3/2})$ Transition by Energy Transfer from $O_2(a^1\Delta_g)$ Generated by a Microwave Discharge in a Subsonic Flow Reactor," *Appl. Phys. Lett.* **86**, 051105 (2005).
13. Verdeyen, J. T., Carroll, D. L., King, D. M., Laystrom, J. K., Benavides, G. F., Zimmerman, J. W., Woodard, B. S., and Solomon, W. C., "Continuous-wave laser oscillation in subsonic flow on the 1315 nm atomic iodine transition pumped by electric discharge produced $O_2(a^1\Delta)$," *Appl. Phys. Lett.*, **89**, 101115 (2006).
14. Hicks, A., Tirupathi, S., Jiang, N., Utkin, Yu., Lempert, W. R., Rich, J. W., and Adamovich, I. V., "Design and operation of a supersonic flow cavity for a non-self-sustained electric discharge pumped oxygen-iodine laser," *J. Phys. D: Appl. Phys.*, **40**, 1408-1415 (2007).
15. Benavides, G. F., Zimmerman, J. W., Woodard, B. S., Palla, A.D., Carroll, D. L., Verdeyen, J. T., King, D. M., Laystrom, J. K., Field, T. H., and Solomon, W. C., "Hybrid Electric Oxygen-Iodine Laser Performance Enhancement and Measurements, Presented at 10th DEPS Symposium, 5-8 Nov. 2007, Huntsville, Alabama (2007).
16. Rakhimova, T. V., Kovalev, A. S., Klopovsky, K. S., Lopaev, D. V., Mankelevich, Yu. A., Vasilieva, A. N., Braginsky, O. V., Popov, N. A., Proshina, O. V., Rakhimov, A. T., "Experimental and theoretical study of a pressure scaling possibility of vhf singlet oxygen generator." *36th AIAA Plasmadynamics and Lasers Conference*, AIAA paper 2005-4918 (2005).
17. Rakhimova, T. V., Kovalev, A. S., Lopaev, D. V., Proshina, O. V., Mankelevich, Yu. A., Vasilieva, A. N., Braginsky, O. V., Klopovsky, K. S., Popov, N. A., Rakhimov, A. T., Kolobyanin, Yu. V., "Pressure scaling of an electro-discharge singlet oxygen generator (ED SOG)." *Gas Flow, Chemical Lasers, and High-Power Lasers*, SPIE paper 634608-1 (2006).
18. Braginsky, O. V., Kovalev, A. S., Lopaev, D. V., Proshina, O. V., Rakhimova, T. V., Rakhimov, A. T., Vasilieva, A. N., "Pressure scaling of an electro-discharge singlet oxygen generator (ED SOG)." *J. Phys. D.: Appl. Phys.*, **40** 6571-6582 (2007).
19. Braginsky, O. V., Vasilieva, A. N., Klopovsky, K. S., Kovalev, A. S., Lopaev, D. V., Proshina, O. V., Rakhimova, T. V., Rakhimov, A. T., "Singlet oxygen generation in O_2 flow excited by RF discharge: I. Homogeneous discharge mode: α -mode." *J. Phys. D.: Appl. Phys.*, **38**, 3609-3625 (2005).
20. Braginsky, O. V., Vasilieva, A. N., Kovalev, A. S., Lopaev, D. V., Mankelevich, Yu. A., Rakhimova, T. V., Rakhimov, A. T., "Singlet oxygen generation in O_2 flow excited by RF discharge: II. Inhomogeneous discharge mode: plasma jet." *J. Phys. D.: Appl. Phys.*, **38**, 3626-3634 (2005).
21. Levitskii, S. M., *Sov. Phys. Tech. Phys.* **2**, 887 (1958).
22. Raizer, Yu. P., *Radio Frequency Capacitive Discharges*. Boca Raton, CRC Press.
23. Yatsenko, N. A., *Zh. Tekh. Fiz.* **51**, 1195 (1981).
24. Vidaud, P., Durrani, S. M. A., and Hall, D. R., *J. Phys. D.* **21**, 57 (1988).
25. Odorobina, I. and Kando, M., *Plasma Sources Sci. Technol.* **5**, 517-522 (1996).
26. L. G. Piper, G. E. Caledonia, and J. P. Kennealy, *J. Chem. Phys.* **75**, 2847 (1981).
27. Rosen, B. "Spectroscopic Data Relative to Diatomic Molecules." Pergamon Press (French), 424-425 (1970).
28. J.W. Zimmerman, D.M. King, A.D. Palla, J.T. Verdeyen, D.L. Carroll, J.K. Laystrom, G.F. Benavides, B.S. Woodard, W.C. Solomon, W.T. Rawlins, S.J. Davis, and M.C. Heaven, "Important kinetic effects in the hybrid ElectricOIL system." *SPIE Vol.* **6261**, 62611R (2006).